Degradation of acetamiprid using graphene-oxide-based metal (Mn and Ni) ferrites as Fenton-like photocatalysts

Asma Tabasum, Ijaz Ahmad Bhatti, Nimra Nadeem, Muhammad Zahid, Zulfiqar Ahmad Rehan, Tajamal Hussain and Asim Jilani

ABSTRACT

This study aims to explore the photocatalytic potential of graphene-oxide-based metal ferrites for the degradation of acetamiprid (an odorless neonicotinoid pesticide). Metal (Mn and Ni) ferrites (along with their graphene oxide composites) were prepared by the hydrothermal method while graphene oxide (GO) was synthesized using a modified Hummer's method. The composites were characterized by scanning electron microscopy, X-ray diffraction, X-ray photoelectron spectroscopy, and Fourier transform infrared spectroscopy. The photocatalysts were studied for their Fenton-like advanced oxidation process to degrade acetamiprid. The composites showed excellent activity against acetamiprid degradation (>90%) in 60 min under UV irradiation. The detailed optimization study was carried out to investigate the influential variables (such as pH, catalyst dose, pollutant concentration, irradiation time, oxidant dose, etc.) to achieve enhanced degradation efficiency. Moreover, the findings were endorsed by central composite design (CCD). It was concluded that degradation was enhanced in an appropriate combination of photocatalyst and hydrogen peroxide. The magnetic character of the metal ferrites and their composites played an important role in the easy separation and reusability of these materials. The present findings result in highly effective, easy to handle and stable heterogeneous photo-Fenton materials for wastewater remediation.

Key words | central composite design (CCD), magnetic graphene oxide, $MnFe_2O_4$, $NiFe_2O_4$, pesticide, wastewater treatment

Asma Tabasum
Ijaz Ahmad Bhatti
Nimra Nadeem
Muhammad Zahid (corresponding author)
Department of Chemistry,
University of Agriculture,
Faisalabad 38040,
Pakistan
E-mail: *rmzahid@uaf.edu.pk*;
zahid595@gmail.com

Zulfiqar Ahmad Rehan
Department of Polymer Engineering,
National Textile University,
Faisalabad,
Pakistan

Tajamal Hussain
Institute of Chemistry,
University of the Punjab,
Lahore
Pakistan

Asim Jilani
Center of Nanotechnology,
King Abdul-Aziz University,
Jeddah 21589,
Saudi Arabia

INTRODUCTION

Keeping in view the easy accessibility of clean water complying with WHO-standards, there is a strong need for developing effective water treatment technologies. Various physico-chemical and biological pre-treatments are currently used. Such treated water normally meets the legal requirements for discharge into water streams. Pesticides and drugs are among the major micro-pollutants found in urban secondary effluents (Al Aukidy *et al.* 2012; Bueno *et al.* 2012; Cabeza *et al.* 2012). Their low concentrations in aqueous streams threaten their inhabitants, owing to bio-accumulation in the muscular tissues of living creatures. Consequently, an effective, economical and eco-friendly treatment is now vital to cope with the recalcitrant chemicals. Pesticides are among the priority pollutants, specifically in countries that are developing agriculturally. Farmers usually spray pesticide formulations in excess onto the crops to raise the product quality and minimize the insect damage. The adsorbed pesticides become part of wastewater when fruits and vegetables are washed in the industry's food processing unit. Acetamiprid (ACTM) is a commonly used neonicotinoid insecticide, being sprayed on citrus fruit (Garcia-Reyes *et al.* 2008). ACTM is chronically as well as an acutely toxic and may cause cancer (Li *et al.* 2010).

The wastewater treatment processes such as adsorption, membrane filtration, biodegradation are usually inefficient for the complete removal/degradation of aquatic pollutants. Advanced oxidation processes (AOPs) have been proved as successful substitutes for these inefficient and costly techniques (Tabasum *et al.* 2019). *In-situ* generated highly reactive hydroxyl radicals (oxidation potential of 2.8 V), are non-selective oxidative species (Konstantinou *et al.* 2014). The photo-Fenton process is among the most effective pollutant-remediation AOPs (Klamerth *et al.* 2013).

doi: 10.2166/wst.2020.098

Generation of radicals and their attack on pollutants play a key role in the degradation process, and light assists the generation of electron/hole pairs as well as keeping photocatalysts in cycle (active) (Pignatello *et al.* 2006; Pérez *et al.* 2018; Nadeem *et al.* 2020).

Different metal-based photocatalysts have been used, and the most widely studied is TiO_2. This study evaluates the catalytic power of manganese and nickel ferrites. Compared to TiO_2, these small sized metal ferrites are more easily separated from aqueous solutions, owing to their magnetic properties (Yu *et al.* 2019). For instance, manganese and nickel ferrites offer narrow band gaps and are fairly stable. But the usability of pure metal ferrites is hindered by the quick recombination of electron-hole pairs. The use of composites, with carbonaceous materials as a support, is an effective strategy to eradicate this problem.

Graphene is a two-dimensional assembly of sp^2 hybridized, covalently linked carbon atoms, with a larger surface area, electrically conductive properties, remarkable adsorptive nature, and excellent thermal stability. Graphene offers charge migration from one active site to another through its electrically conductive surface, which inhibits the electron-hole pair recombination and accelerates the process of catalysis (Zhang *et al.* 2010; Li *et al.* 2018).

In view of all of this, many attempts have been made to prepare hybrids with different materials to degrade pollutants (Xiang *et al.* 2012; Zahid *et al.* 2019). Composites of manganese and nickel ferrites with graphene oxide (GO) have been prepared and used extensively for adsorption of heavy metals (Kumar *et al.* 2014; Naushad *et al.* 2017). For example, the degradation of NH_3 using graphene manganese ferrite has been reported under visible light irradiations. The degradation efficiency of composite was found to be 92.0% using H_2O_2 as an oxidizing agent (Zhou *et al.* 2016). Further, the high reaction rate ($0.01443\ min^{-1}$) of rGO-$MnFe_2O_4$ composites as compared to pristine $MnFe_2O_4$ ($0.00248\ min^{-1}$) for photocatalytic degradation of methylene blue demonstrates the significant role of reduced graphene in photocatalytic activity enhancement (Huang *et al.* 2019).

This study focused on the simple approach to synthesizing magnetic metal (manganese and nickel) ferrites and their graphene-oxide-based hybrids. The prepared composites were characterized using Fourier transform infrared spectroscopy (FTIR), scanning electron microscopy (SEM), X-ray powder diffraction (XRD), and X-ray photoelectron spectroscopy (XPS), and investigated for their photocatalytic potential in terms of degradation of ACTM in UV light. To study the effective role of various process parameters (such as pH, catalyst dose, pollutant concentration, oxidant dose and irradiation time), the process of ACTM's degradation was also evaluated using central composite design.

MATERIALS AND METHODS

Materials

Graphite powder (<45 μm, ≥99.99%), iron(III) chloride hexahydrate (99.0%) and manganese (II) chloride (99.0%) were purchased from Daejung Chemicals and Metals, Korea. Sodium nitrate (≥99.0%), sulphuric acid (clear, assay: 98.0%), hydrogen peroxide (30% w/w), iron (II) sulphate heptahydrate (≥98.0%) and sodium hydroxide (≥99.9%) were purchased from Sigma-Aldrich, USA). The technical grade (≥97%) pesticide sample, ACTM, was obtained from the local pesticide manufacturer in Pakistan. All chemicals were analytical grade and used as received without further purification. Distilled water was used throughout the study.

Synthesis of catalyst and characterization

GO was synthesized by following the modified Hummer's method (Tabasum *et al.* 2019) using graphite powder. GO-MFe_2O_4 (where M = Mn, Ni) was prepared following the one-pot hydrothermal method in the presence of GO suspension (Yao *et al.* 2014). Dispersion of GO (10% of MFe_2O_4 mass used) was made using an ultrasonic bath in 10.0 mL of distilled water. Afterward, metal (Ni or Mn) chloride and $FeCl_3.6H_2O$, in a 1:2 mole ratio, were dissolved in 15 mL distilled water. Both the solutions were mixed under constant stirring. NaOH solution (0.1 molar) was carefully added to the mixed solution while keeping the reaction vessel on the magnetic stirrer until the pH reached 11 at ambient temperature. The final total volume of suspension was made up to 60 mL by adding the requisite amount of distilled water; it was then transferred into a 100 mL sealed Teflon-lined stainless-steel autoclave reactor and kept at 180 °C for 14 hours. GO-MFe_2O_4 particles were separated from the parent solution magnetically and rinsed with distilled water until the pH was neutral, and they were then washed thoroughly with ethanol. Finally, a magnetic powder was obtained after drying these magnetic particles at 65 °C. For comparative study, pure MFe_2O_4 particles were also synthesized separately via an analogous method without GO addition.

Morphological study and micro-structural analysis of the samples were performed using an SEM (JSM-5910 JEOL, Japan). Structural analysis of prepared metal ferrites and their composites with graphene oxide was done on a Bruker AXS D8-advance powder X-ray diffractometer with Cu-Kα radiation ($\lambda = 1.5418$ Å), with the scan speed at 2^0/min. Interaction among the various functional groups within the composite was determined by FTIR spectrometer (Thermo Nicolet). The surface chemical composition and elemental analysis of catalysts were conducted by XPS (Escalab 250 XPS system, Thermo Fisher Scientific UK).

Catalytic degradation experiment

Photocatalytic degradation of ACTM was investigated following similar protocols described previously (Tabasum *et al.* 2019). The homogeneity of the suspension was assured using an orbital shaker placed in appropriate light (in a UV chamber). The UV intensity was measure using a UV radiometer (UVX; UVP with 254 nm probe). All the tests were performed at ambient temperature ($25 \pm 2\,^{\circ}C$). After the specific irradiation time, the catalysts were thoroughly washed with water, dried and kept for further investigation (relevant to its reusability potential). The residual ACTM in solution was estimated after measuring absorbance using a double beam spectrophotometer (Cecil 7200, UK) at 245 nm (λ_{max} for ACTM). The untreated ACTM solution was taken as the control, to determine the percentage degradation efficiency of the system. The effect of experimental parameters was studied and optimized systematically in different ranges of pH (2–8), oxidant/H_2O_2 dose (1.16–58 mM), catalyst dose (0–200 mg/L), ACTM conc. (2–16 ppm) and irradiation time (15–120 min).

Experimental design for RSM

The simultaneous interactions of influencing parameters were studied using central composite design (CCD) of response surface methodology (RSM). Three chosen factors for CCD were oxidant dose (X_1), catalyst dose (X_2) and ACTM concentration (X_3). Ranges of these independent variables along with their levels (three for each) are shown in Table 1.

Percentage degradation was the chosen dependent variable (output), designated by 'Y'. The model followed the following general quadratic equation:

$$Y = \beta_0 + \sum_{i=1}^{n} \beta i Xi + \sum_{i=1}^{n} \beta ii Xi^2 + \sum_{i=1}^{n-1} \sum_{j=i+1}^{n} \beta ij\, Xi\, Xj$$

Here Y is the predicted percentage degradation efficiency; β_0, β_i, β_{ii} and β_{ij} are designated to offset the term (linear/quadratic) and interaction coefficients for Xi and Xj as independent variables. Triplicate runs were performed for each experimental trial. Statistical analysis was performed using design expert 7.0.0 software and fitted to the polynomial regression model. The fitness of the model was tested using analysis of variance (ANOVA). Computation of F-value (at 0.05 probability value) gave a measure of the parameters' significance in terms of linear and interactive effects.

RESULTS AND DISCUSSION

Synthesis and structural characterization of catalysts

The formation GO-MFe_2O_4 composites can be explained in three consecutive steps. (1) First of all, when two metal precursors were homogenized in the exfoliated GO suspension, they were adsorbed and co-ordinated through specific oxygen-containing groups (carboxyl, epoxy and hydroxyl groups) located on GO. These functional groups are anchor sites that assist adsorption/*in-situ* deposition of metal ions (Mn^{2+}, Ni^{2+}/Fe^{3+}) onto GO sheets. (2) Agitation of the mixture at basic conditions assisted the adsorbed metal ions to hydrolyze and transform into their respective

Table 1 | Values of independent variables used in CCD

			Actual levels of coded variable (GO-$MnFe_2O_4$)			Actual levels of coded variable (GO-$NiFe_2O_4$)		
Process variables	**Units**	**Symbols**	**−1**	**0**	**+1**	**−1**	**0**	**+1**
A-Oxidant concentration	(mM)	X_1	2.9	26.82	50.75	14.5	36.25	58
B-Catalyst dose	(mg/L)	X_2	20	110	200	20	110	200
C-ACTM load	(ppm)	X_3	4	10	16	4	10	16

hydroxides $M(OH)_2/M(OH)_3$. (3) Thermal treatment at 180 °C for 14 hours helped these metal hydroxide clusters to be condensed in the form of MFe_2O_4 nuclei. This was the stage at which prepared ferrites oriented themselves in specific dimensions so that their coercivity was improved. Further growth and nucleation of MFe_2O_4 was due to redox reactions under basic conditions and at elevated temperature. In this way, stable GO-MFe_2O_4 composites were formed. The whole process can be summarized in simple chemical reactions as:

$$MCl_2 \cdot 6H_2O + 6NaOH \xrightarrow{-2NaCl,\ -6H_2O} M(OH)_2 \longrightarrow MO$$

$$2FeCl_3 \cdot 6H_2O + 6NaOH \xrightarrow[-12H_2O]{-6NaCl} 2Fe(OH)_3 \longrightarrow Fe_2O_3 + 3H_2O$$

$$MO + Fe_2O_3 \xrightarrow{180°C} MFe_2O_4$$

The morphology of graphene oxide and its composites with metal ferrites is shown in Figure 1. The SEM images of graphene oxide show the high surface area, which contributes in its pronounced adsorptive property for oxidants as well as for pesticide molecules. Ferrite particles firmly anchored onto GO sheets and contributed towards enhanced durability, magnetic separation, and reduced catalyst leaching during the degradation process. The SEM images clearly show how the ferrite molecules were fabricated onto GO. The composite formation not only immobilized the magnetic ferrite particles but also assisted in preventing their agglomeration.

The structural analysis of ferrite samples was done by XRD; the patterns were analyzed and indexed using powder X software (Bai *et al.* 2012). Results of XRD analysis of GO, $MnFe_2O_4$, $NiFe_2O_4$, GO-$MnFe_2O_4$ and GO-$NiFe_2O_4$ are shown in Figure 2(a) and 2(b). The XRD patterns of GO showed a strong peak at $2\Theta = 10.7°$, corresponding to the (002) inter-planar spacing. No further peaks indicated that no unreacted or unoxidized graphene was present in the sample.

As both the ferrites are mixed oxides of transition metals (Mn and Ni), occupying tetrahedral or octahedral positions in the crystal lattice, different diffraction peaks are assigned to each ferrite, which reflects various crystal planes i.e. diffraction peaks at 2Θ equals to 29.7°, 34.9°, and 61.6° could be indexed to pure phase spinel $NiFe_2O_4$. The XRD results confirm the successful synthesis of composites (GO-$MnFe_2O_4$ and GO-$NiFe_2O_4$) using the one-pot hydrothermal method (Zhou *et al.* 2010).

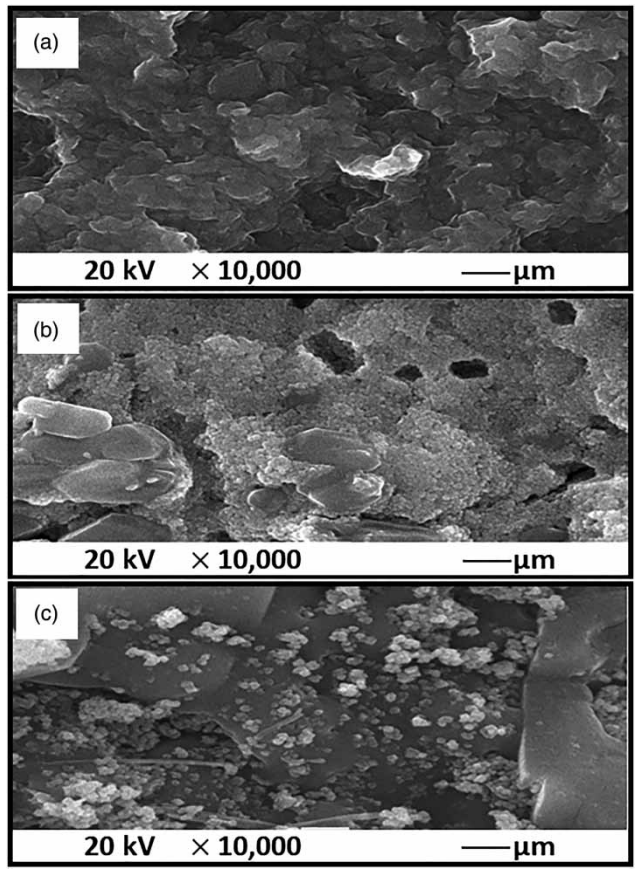

Figure 1 | SEM images of prepared samples: (a) graphene oxide, (b) GO-$MnFe_2O_4$ and (c) GO-$NiFe_2O_4$.

Electronic absorption by composites and their constituent metal ferrites in the infra-red region are shown in Figure 3(a) and 3(b). FTIR spectra help in elucidating the chemical bonding and interactions when composites are being formed. Spectra of both the composites show the differences in bands throughout the region of 3,500–900 cm^{-1}. The two absorption bands that appear below 900 cm^{-1} justify the formation and presence of metal ferrites, as they are characteristic of ferrites. For instance, the band at 582 cm^{-1} is attributed to Fe-O stretching vibrations in metal ferrites (Qi *et al.* 2019). In another way, these bands appear because of lattice vibrations of oxide ions against their respective cations, present in a ferrite crystal. In ferrite samples, the absorptions near 1,642 cm^{-1} and 3,392 cm^{-1} are attributed to vibrations of bonded hydroxyl groups as well as deformation of water molecules (Yu *et al.* 2016). The three peaks at 3,424 cm^{-1}, 1,642 cm^{-1}, and 1,037 cm^{-1} show the presence of GO. Since the spectra of both composites reveal that their compositional GO gave a broad band near 3,424 cm^{-1}, attributed to stretching vibrations of GO

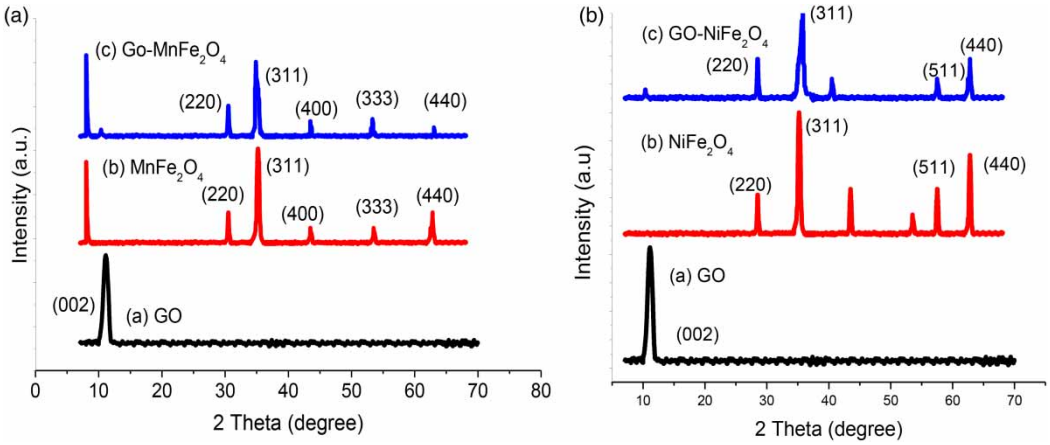

Figure 2 | XRD patterns of (a) GO, $MnFe_2O_4$ and GO-$MnFe_2O_4$, (b) GO, $NiFe_2O_4$ and GO-$NiFe_2O_4$.

structural hydroxyl groups. The band near 1,642 suggests C = O stretching vibrations in attached carboxylic groups (Liu *et al.* 2017). The sharpness, intensity and red-shifted positions of bonds reflect strong chemical interaction among Fe-O-C bonds, i.e. C = O stretching vibration peak (of the carboxylic group) near 1,642 cm^{-1} and 3,392 cm^{-1}, attributed to the complex linkage of COO- with iron in Fe_3O_4. Formation of Fe-O-C bond confirmed the proper crystal growth, nucleation, and impregnation of magnetite on active sites of GO. Thus, from FTIR results it can be inferred that ferrite particles were firmly anchored on the GO surface.

The surface chemical composition of the graphene-based photocatalyst has a vital role as most of the reaction occurs over the surface of the composites (Jilani *et al.* 2017, 2018a). The surface compositional analysis of the prepared ferrite samples was investigated through XPS. Figure 4(a) shows the surveyed surface composition of $NiFe_2O_3$ and GO-$NiFe_2O_3$ while Figure 4(b) shows the elements detected and their respective atomic percentages. The surface compositions revealed the presence of O 1s, Fe 2p3, Ni 2p, and C 1s, which shows the simplicity and accuracy of the synthesis method. The $NiFe_2O_4$ has 76.7% of O 1s and 21.5% and 1.8% of Fe 2p3 and Ni 2p respectively. Moreover, the presence of C 1s (21%) was observed in the case of GO-NiF_2O_4, which indicates the successful incorporation of GO into NiF_2O_4. However, GO has affected the elemental composition of the $NiFe_2O_4$ as shown in Figure 4(b). This change in the composition can enhance the photocatalytic activity of GO composite materials (Jilani *et al.* 2018a, 2018b).

The survey of the surface composition of MnF_2O_4 and GO-$MnFe_2O_4$ (Figure 4(c)) also confirmed the presence of GO with C 1s (29.7%). The Fe 2p3 was about 15.0% and 15.3% for $MnFe_2O_4$ and GO-$MnFe_2O_4$ respectively.

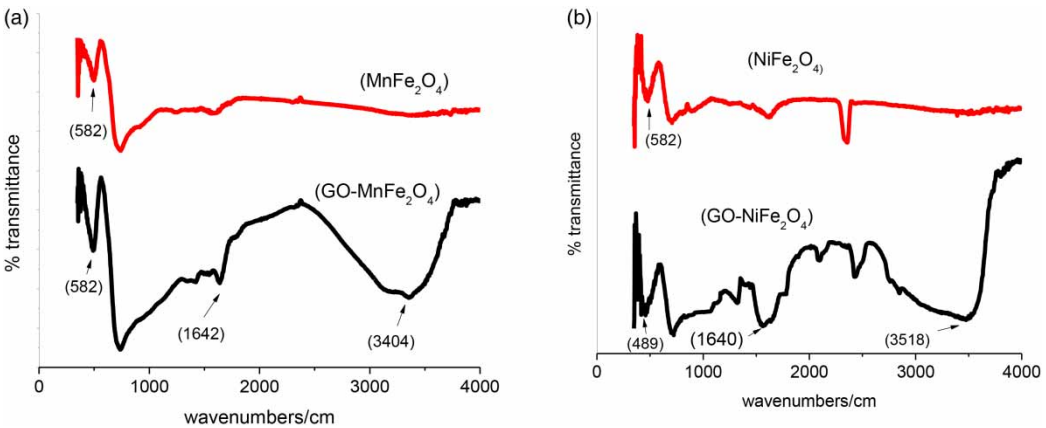

Figure 3 | FTIR spectra of (a) $MnFe_2O_4$ and GO-$MnFe_2O_4$, (b) $NiFe_2O_4$ and GO-$NiFe_2O_4$.

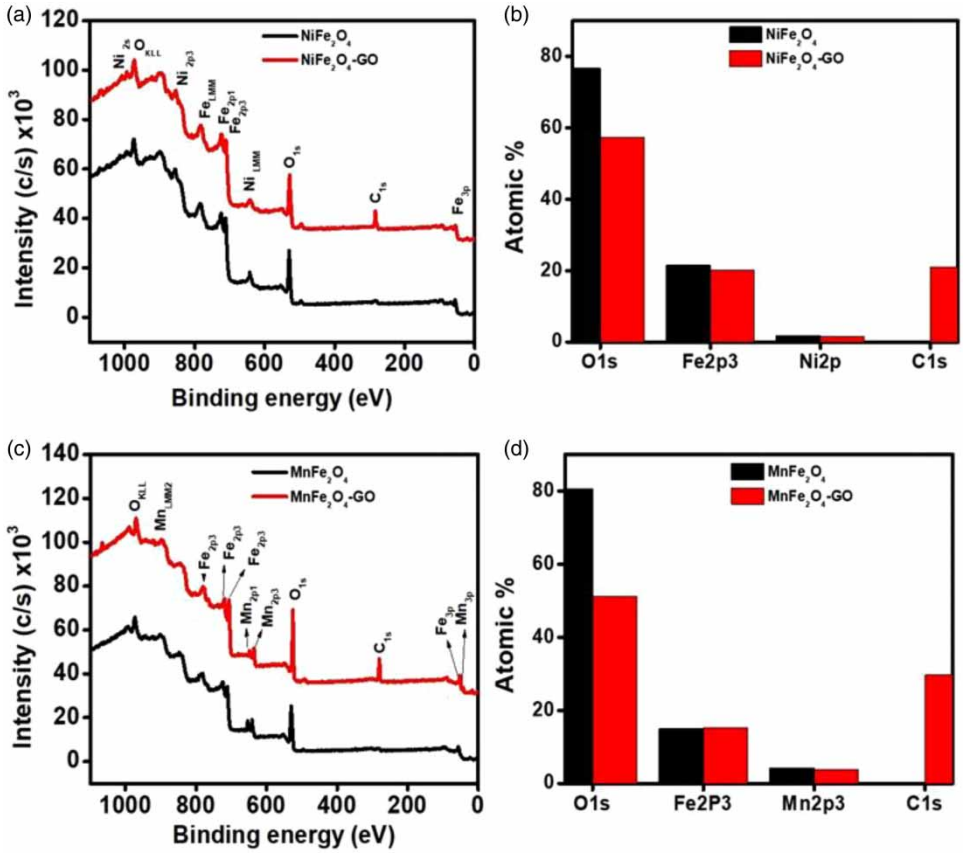

Figure 4 | XPS analysis (a) and (c) survey spectra and (b) and (d) detected compositions of $MnFe_2O_4$ and $NiFe_2O_4$ ferrite and their GO-based composites.

The O 1s was about 80.7% and 51.1% for $MnFe_2O_4$ and GO-$MnFe_2O_4$ respectively. The complete composition of detected elements in the case of $MnFe_2O_4$ and GO-$MnFe_2O_4$ is concisely shown in Figure 4(d).

Effect of various parameters on the degradation of ACTM

Effect of pH

As heterogeneous photocatalysis is a surface linked phenomenon and the pH of the solution greatly affects superficial charge distribution on the catalyst's surface, it is important to investigate the effect of varying the pH of the solution on catalytic potential. The pH range of 2 to 8 was investigated in the heterogeneous photo-Fenton process for ACTM's degradation and the results are shown in Figure 5. It is evident from Figure 5(a) that degradation efficiencies (for all catalysts, ferrites and their GO composites) were pH dependent. Acidic pH (pH = 3) favored the degradation of ACTM and degradation rate gradually decreased as the conditions were shifted to alkaline pH. This is because pH determines the charge properties of the catalyst's surface. In acidic conditions, the catalyst's surface became protonated and the ^{-}OH ions, generated in an aqueous system, could accelerate oxidant decomposition. The decomposition of oxidant molecules generates hydroxyl radicals, which non-selectively attack pollutant molecules. On the other hand, in alkaline conditions, the surface of the catalyst became deprotonated and therefore negatively charged, with no enhanced production of reactive hydroxyl radicals, resulting in decreased ACTM degradation (Ren *et al.* 2012).

Furthermore, in an alkaline solution of ACTM, there was a greater likelihood of the reaction between ferrous ions and hydroxyl ions (present in excess), which would account for the lower degradation rate. Consequently, brownish sludge formed on the surface of catalysts, which not only blocked active sites but also hindered light penetration (Aleksić *et al.* 2010). The solubility product constant for $Fe(OH)_2$ is 1.8×10^{15}, thus fewer hydroxyl radicals and iron ions were available for the Fenton reaction (Pignatello *et al.* 2006; Soto *et al.* 2018).

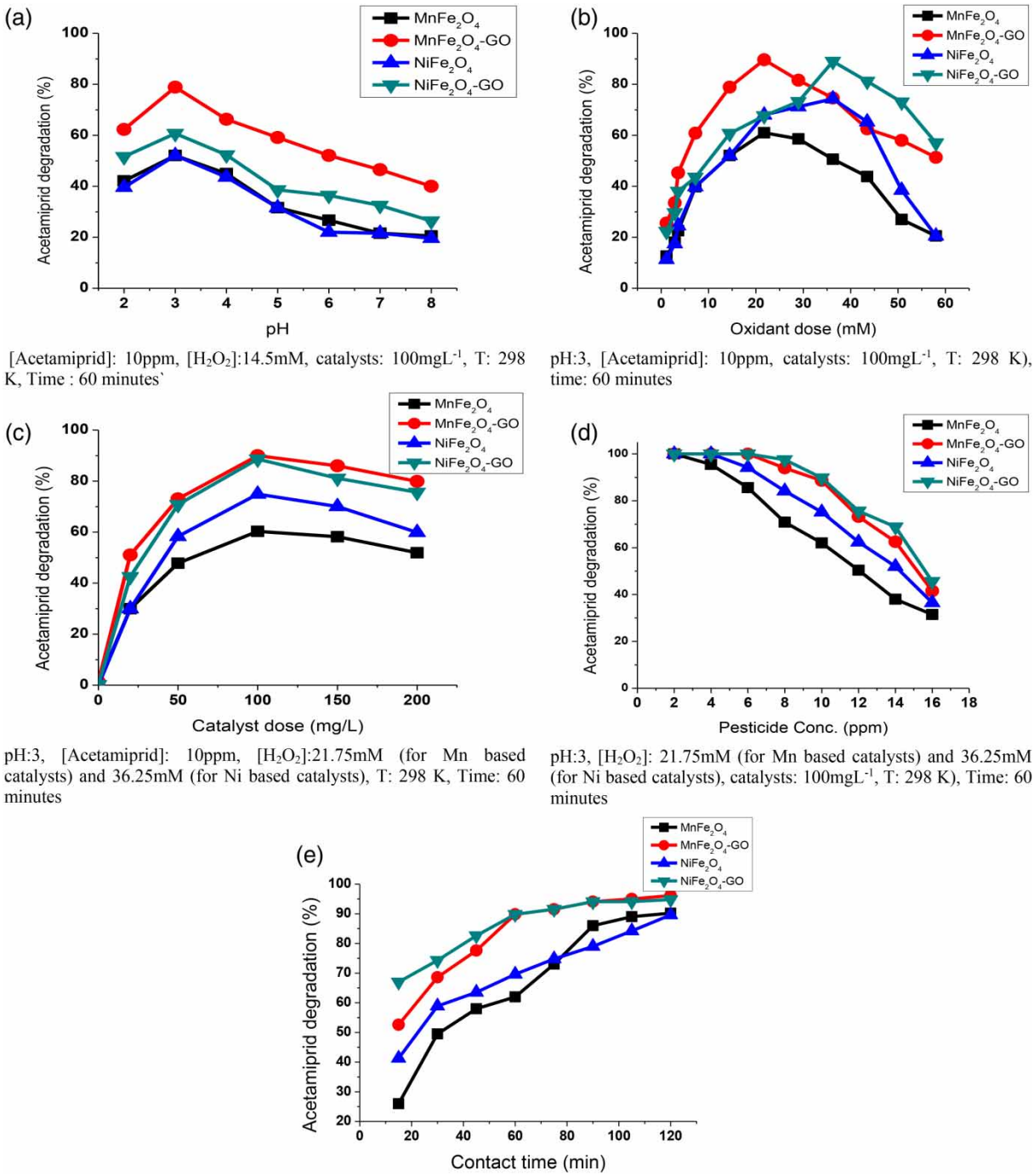

[Acetamiprid]: 10ppm, [H_2O_2]:14.5mM, catalysts: 100mgL^{-1}, T: 298 K, Time : 60 minutes`

pH:3, [Acetamiprid]: 10ppm, catalysts: 100mgL^{-1}, T: 298 K), time: 60 minutes

pH:3, [Acetamiprid]: 10ppm, [H_2O_2]:21.75mM (for Mn based catalysts) and 36.25mM (for Ni based catalysts), T: 298 K, Time: 60 minutes

pH:3, [H_2O_2]: 21.75mM (for Mn based catalysts) and 36.25mM (for Ni based catalysts), catalysts: 100mgL^{-1}, T: 298 K), Time: 60 minutes

Figure 5 | Effect of various parameters on ACTM degradation: (a) pH, (b) oxidant dose, (c) catalyst load, (d) pesticide concentration and (e) contact time.

Effect of oxidant dose

Oxidant dose is also an important parameter for the efficient pollutant degradation process in the Fenton-based advanced oxidation reaction. A catalyst's enhanced efficiency lies in an appropriate catalyst to oxidant ratio. The impact of varying concentrations of hydrogen peroxide, as the oxidant, was studied in the range of 1.16–58 mM and the results are shown in Figure 5(b). Oxidant concentration on very high or low values normally disturbed the balance of the Fenton process, as evident from Figure 5(b). It is clear from the experimental results that the addition of 21.75 mM (in the

case of $MnFe_2O_4$) and 36.25 mM (for $NiFe_2O_4$) was enough to enhance photocatalytic activity to 60–80%.

Beyond this value up to 58 mM, excess hydrogen peroxide molecules would not participate in the oxidative degradation of pollutants. At higher H_2O_2 concentrations, these molecules react with each other to form another oxidative radical (the peroxyl radical). The oxidative potential of peroxyl radicals is lower than that of hydroxyl radicals. An increase in the oxidant dose up to the optimum value enhanced pesticide degradation because it was able to activate the surface-bound active sites. On the other hand, H_2O_2 in excess scavenged the produced hydroxyl radicals, making them unavailable for the oxidative reaction, because the hydroxyl radicals are transformed into hydro-peroxyl radicals ($HOO^{\cdot}$) (Yu *et al.* 2016). Moreover, H_2O_2 molecules also compete with the ACTM molecules for adsorption (catalytic) sites bound to the surface of catalyst (Titouhi & Belgaied 2016).

Effect of catalyst dose

The surface of a catalyst provides reaction sites to degrade pollutant molecules so varying catalyst concentration greatly affects the overall efficiency of the degradation process. The effect of varying catalyst dose was investigated in the range of 0–200 mg/L and the results are shown in Figure 5(c). It is evident from the figure that the maximum catalytic degradation was found at 100 mg/L of catalyst concentration. The higher the amount of catalyst, the more active sites will be provided. These active sites facilitate the enhanced production of activators (hydroxyl radicals) as well as the adsorption of the pollutant molecules.

However, the degradation efficiency declined at a higher concentration of catalysts because of the catalyst's agglomeration. Resultantly, catalyst particles stack over each other, leaving active sites unavailable for the Fenton reaction to proceed (Hoque & Guzman 2018). Also, at higher catalyst doses, light is unable to penetrate the solution for the photo-Fenton reaction, which decreases the photo-catalytic potential. Thus, the rate of production of hydroxyl radicals is decreased. Besides this, scavenging of produced –OH radicals by excess catalyst species occurs (in case of higher catalyst doses) and thus terminates the degradation process. Figure 5(c) also shows that the photo-Fenton efficiency would not be disturbed even at a high dosage of catalyst in the presence of GO-ferrite composites. The GO not only facilitated the ferrites with conductive support but also prevented the catalysts from agglomerating (Mirzaei *et al.* 2017).

Effect of acetamiprid concentration

The effect of pesticide concentration was studied in a range from 2 to 16 ppm. The results are presented in Figure 5(d) and show that pesticide is efficiently degraded (more than 85%) in the case of GO-ferrite composites for up to 10 ppm pesticide concentration. However, with further increases in pesticide concentration, the degradation efficiency is continuously decreased. It is justified by the fact that at this stage (ACTM $\leq$ 10 ppm) limited target molecules are being adsorbed and catalyzed by more available active sites, so the catalytic potential of the system is remarkable. Further addition of pollutant (ACTM > 10 ppm) lowers the catalytic degradation efficiency by making the ACTM molecules stay in the solution (due to lack of available active sites). This gives no space for the reactions responsible for the formation of surface-bound reactive oxygen species (Tabasum *et al.* 2019).

Another reason is that the high concentration of pesticide molecules absorbs more photons, which in turn decreases the number of photons available for photocatalytic reaction. In other words, the transparency of the solution is greatly affected. Moreover, with the increase in pesticide load, the oxidant to pollutant ratio is reduced, which has a negative impact on photocatalytic degradation (Luo *et al.* 2010).

Effect of UV irradiation time

The irradiation time for UV light ($\lambda = 254$ nm) on the degradation of ACTM solution at optimized conditions was studied for continuous monitoring of degradation efficiency for 120 min. The present study is advantageous as compared to previously reported research using similar material (Yamaguchi *et al.* 2017), that 60 min of reaction time (under UV irradiations) was enough for almost complete degradation of ACTM. Further, UV irradiation was found to be the most important factor along with prepared material for the efficient degradation of pesticides. The results show (Figure 5(e)) that pesticide degradation increased sharply during the first 60 min. Over time, the rate of the ACTM degradation reaction slowed. The active sites located on the catalyst's surface need a specific period to degrade the adsorbed pollutant molecules. Hydroxyl ions are furnished from the aqueous pesticide solution, affecting the pH directly and the rate of catalysis indirectly. These generated -OH ions also reacted with bivalent ions and hence suppressed the Fenton reaction. Moreover, with time, hydrogen peroxide became the

limiting reactant because the recommended stoichiometric amount of hydrogen peroxide was depleted (Velichkova *et al.* 2013).

Reusability (stability) of catalyst and iron leaching

Under optimized conditions, the stability of the catalysts was verified by conducting successive trials of the repeatedly used catalysts (see Table 2). To do so, used the catalysts were separated from the treated ACTM solution by applying an external magnetic field, then rinsed three times with distilled water, dried in the oven at 60 °C, weighed and investigated for their catalytic potential against the pesticide solution. All the reusability trials were run at the optimized conditions, i.e. the pH of reaction media was 3, the H_2O_2 concentration was 21.75 mM (for Mn based catalysts) and 36.25 mM (for Ni based catalysts), the catalyst dose was 100 mgL^{-1}, the ACTM concentration was 10 ppm and the temperature was 298 K. There was no significant loss in catalytic activity after five consecutive runs; approximately 5–10% decrease in catalytic activity was observed.

The values of iron leaching after each run were measured using an atomic absorption spectrometer. Iron leaching was also far below the range suggested by European Union directives (2.0 mg/L). The concept of heterogeneous catalysis has evolved owing to heavy iron leaching during the homogeneous catalytic process. Feasible application of heterogeneous Fenton catalysts in wastewater treatment requires that they should be stable in terms of metal leaching from the solid to the liquid phases. Gradual and continuous metal leaching leads to the deactivation of catalysts with further pollution of water. Leaching studies give us a better insight into the elucidation of degradation mechanisms. The interionic forces of attraction are weaker in the case of ferrous and oxide ions in the lattice, so monitoring the stability of Fe^{2+} is more important. The reduction of ferric ions to ferrous ions is the time when there are more chances of iron leaching (Xu *et al.* 2007). From Table 2, it can be seen that iron leaching is quite low after five consecutive cycles, indicating the mechanism to be heterogeneous.

Comparison of various treatment methods

Removal/degradation of ACTM from the aqueous system (either through adsorption or during oxidative degradation) was studied using different catalysts and methodologies. The results are shown in Figure 6, which shows that adsorption of pesticide onto the catalyst's surface could only remove 17% of the ACTM's initial concentration (C_o) after 60 min of contact time. Oxidant dose (36.25 mM) and UV irradiation (for 60 min) alone were also not able to achieve satisfactory degradation of ACTM (less than 15%).

In contrast to the individual use of oxidants, catalysts and UV light, their combination synergistically shifts the degradation reaction from about 15% to 62–68% (roughly

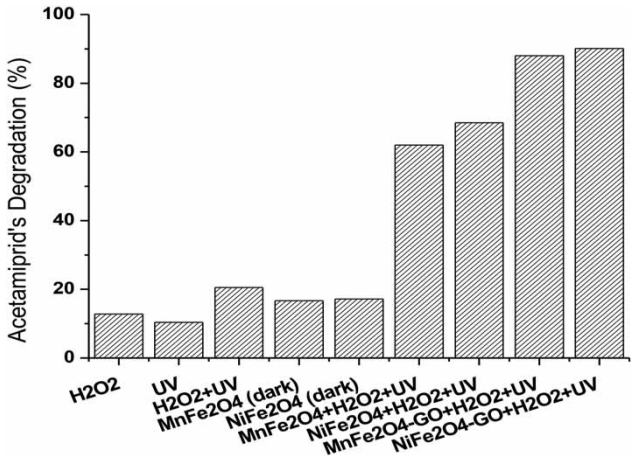

Figure 6 | Catalytic degradation of ACTM under different treatment methods at pH 3, [ACTM] 10 ppm, [H_2O_2] 36.25 mM, catalysts dose 100 mg L^{-1} and irradiation time 60 min).

Table 2 | Stability of catalysts towards the heterogeneous Fenton degradation of acetamiprid

	$MnFe_2O_4$		$GO\text{-}MnFe_2O_4$		$NiFe_2O_4$		$GO\text{-}NiFe_2O_4$	
Run	Degradation (%)	Iron leaching (ppm)	Degradation (%)	Iron leaching (ppm)	Degradation (%)	Iron leaching (ppm)	Degradation (%)	Iron leaching (ppm)
1st	86	1.19	90.2	0.75	75.74	1.46	92	0.89
2nd	79	1.35	89	0.64	72.5	1.41	89	0.95
3rd	75	1.32	85.6	0.61	70.2	1.27	82	0.73
4th	67	1.38	78.9	0.54	65.7	1.02	78	0.66
5th	62	0.574	73.5	0.52	61.01	0.98	71	0.57

As per EU directives, Fe leaching should not be higher than 2.0 ppm.

seven times the individual effect of oxidant and UV light). An extremely positive effect in the ACTM's removal is noticeable (% degradation = 90) when metal ferrites are used in combination with GO. The present study also validates the findings of Fe_3O_4 and GO-Fe_3O_4 described elsewhere (Tabasum *et al.* 2019). The successful utilization of metal (Mn, Ni) ferrite and their GO-based composites for effective degradation of pesticides suggests that these catalysts are as effective as control samples (Fe_3O_4 and GO-Fe_3O_4). ACTM depletion (under the same processes conditions) showed the enhancement of the oxidation reaction by graphene oxide's catalytic support in the GO-ferrite composites. So the catalysts provide a greater number of adsorption sites along with the decrease in electron/hole pair recombination. The generation of more hydroxyl radicals is superficially linked to composites in the presence of GO. Resultantly, the composite's surface becomes more reactive for the degradation of ACTM molecules.

Optimization through response surface methodology

Response surface models were developed by carrying out 20 batch experiments, as per model requirement, for the two GO-based metal ferrite composites. The regression coefficients of polynomial models for the investigated response using GO-$MnFe_2O_4$ and GO-$NiFe_2O_4$ are shown in Table S-1 and Table S-2 in the Supplementary Material, respectively. As depicted in ANOVA, all independent variables possessing p-values less than 0.05, significantly influence the percentage degradation (response). The interactions of the three variables i.e. oxidant concentration (A), catalyst dose (B) and ACTM load (C) was studied. The second-order polynomial equations for the two composites are as follows:

$$\text{ACTM degradation } (\%)_{(\text{using GO}-MnFe_2O_4)} = 90.08 + 4.91^{*}A + 7.55^{*}B - 15.28^{*}C + 1.02^{*}AB + 8.31^{*}AC + 6.88^{*}BC - 18.30^{*}A^2 - 22.79^{*}B^2 - 7.12^{*}C^2$$

$$\text{ACTM degradation } (\%)_{(\text{using GO}-NiFe_2O_4)} = 91.38 + 10.43^{*}A + 18.69^{*}B - 16.12^{*}C + 6.79^{*}AB - 5.31^{*}AC - 4.79^{*}BC - 16.76^{*}A^2 - 17.48^{*}B^2 - 17.98^{*}B^2$$

The analysis of the above polynomial equation reveals that all three factors have a certain influence on degradation reaction, but an appropriate balance should be there between the two catalytic reagents (oxidant concentration and catalyst dose).

The response surfaces showing the interaction of two dependent variables (keeping the third factor fixed at the center level) in terms of the degradation of ACTM is shown in Figure S-1 (Supplementary Material). It has been observed that in the case of oxidant concentration and catalyst dose, the impact of increasing catalyst concentration is more pronounced at higher concentrations because the optimum balance in the ratio between the two variables is significant. In the case of the interaction of oxidant concentration with ACTM load, it has been demonstrated that the degradation efficiency decreases above certain oxidant doses due to a number of factors, such as self-decomposition, scavenging, back reactions, etc. The response surfaces showed the variables are interacting significantly with each other. Hence, the optimum combination of the influencing factors is vital to maintaining the efficient degradation of ACTM.

CONCLUSION

This study deals with the facile synthesis of manganese and nickel ferrite composites using graphene oxide. The impregnation of the metal ferrites onto the GO was successfully validated through SEM, XRD, XPS and FTIR analyses. Composites showed efficient oxidative degradation of ACTM under UV light. The catalytic activity of metal ferrites increased in the presence of graphene oxide, as GO supported the material to enhance durability and reusability of composite with concomitant ease in electron transportation from one active site to another. The combination of metal ferrites with graphene oxide improved catalytic performance of pure metal ferrites by electron/hole pair recombination. Also, it made the catalyst more stable than pure ferrite. The catalysts were reused for five successive runs without significant loss of degradation efficiency. Negligible iron leaching was found, which indicates the stability of the catalysts towards heterogeneous catalytic reaction.

The direct correlation between the ACTM removal with oxidant dose, catalyst dosage, pollutant load, and pH were investigated. The optimum operational conditions for achieving maximum catalytic efficiency (~90%) were pH 3, catalyst dose of 100 mg/L, initial ACTM concentration of 10 mg/L and irradiation time 60 min. The results also reveal that CCD coupled with RSM is a reliable and valuable tool, that helps to optimization of different parameters influencing the rate of pollutant degradation. High catalytic power, strong magnetism for easy separation, extraordinary durability, low iron leaching, and efficient reusability are the salient advantages of GO-based manganese and nickel ferrites.

ACKNOWLEDGEMENTS

The authors would like to acknowledge the Higher Education Commission, Pakistan, for financial support to successfully perform this work.

CONFLICT OF INTEREST

There is no conflict of interest among the authors in relation to this study.

SUPPLEMENTARY MATERIAL

The Supplementary Material for this paper is available online at https://dx.doi.org/10.2166/wst.2020.098.

REFERENCES

Al Aukidy, M., Verlicchi, P., Jelic, A., Petrovic, M. & Barcelò, D. 2012 Monitoring release of pharmaceutical compounds: occurrence and environmental risk assessment of two WWTP effluents and their receiving bodies in the Po Valley, Italy. *Science of the Total Environment* **438**, 15–25.

Aleksić, M., Kušić, H., Koprivanac, N., Leszczynska, D. & Božić, A. L. 2010 Heterogeneous Fenton type processes for the degradation of organic dye pollutant in water – the application of zeolite assisted AOPs. *Desalination* **257** (1), 22–29.

Bai, S., Shen, X., Zhong, X., Liu, Y., Zhu, G., Xu, X. & Chen, K. 2012 One-pot solvothermal preparation of magnetic reduced graphene oxide-ferrite hybrids for organic dye removal. *Carbon* **50** (6), 2337–2346.

Bueno, M. M., Gomez, M., Herrera, S., Hernando, M., Agüera, A. & Fernández-Alba, A. 2012 Occurrence and persistence of organic emerging contaminants and priority pollutants in five sewage treatment plants of Spain: two years pilot survey monitoring. *Environmental Pollution* **164**, 267–273.

Cabeza, Y., Candela, L., Ronen, D. & Teijon, G. 2012 Monitoring the occurrence of emerging contaminants in treated wastewater and groundwater between 2008 and 2010. The Baix Llobregat (Barcelona, Spain). *Journal of Hazardous Materials* **239**, 32–39.

Garcia-Reyes, J. F., Gilbert-Lopez, B., Molina-Diaz, A. & Fernandez-Alba, A. R. 2008 Determination of pesticide residues in fruit-based soft drinks. *Analytical Chemistry* **80** (23), 8966–8974.

Hoque, M. & Guzman, M. 2018 Photocatalytic activity: experimental features to report in heterogeneous photocatalysis. *Materials* **11** (10), 1990.

Huang, X., Liu, L., Xi, Z., Zheng, H., Dong, W. & Wang, G. 2019 One-pot solvothermal synthesis of magnetically separable rGO/$MnFe_2O_4$ hybrids as efficient photocatalysts for degradation of MB under visible light. *Materials Chemistry and Physics* **231**, 68–74.

Jilani, A., Othman, M. H. D., Ansari, M. O., Kumar, R., Alshahrie, A., Ismail, A. F., Khan, I. U., Sajith, V. K. & Barakat, M. 2017 Facile spectroscopic approach to obtain the optoelectronic properties of few-layered graphene oxide thin films and their role in photocatalysis. *New Journal of Chemistry* **41** (23), 14217–14227.

Jilani, A., Othman, M. H. D., Ansari, M. O., Hussain, S. Z., Ismail, A. F. & Khan, I. U. 2018a Graphene and its derivatives: synthesis, modifications, and applications in wastewater treatment. *Environmental Chemistry letters* **16** (4), 1301–1323.

Jilani, A., Othman, M. H. D., Ansari, M. O., Oves, M., Alshahrie, A., Khan, I. U. & Sajith, V. 2018b A simple route to layer-by-layer assembled few layered graphene oxide nanosheets: optical, dielectric and antibacterial aspects. *Journal of Molecular Liquids* **253**, 284–296.

Klamerth, N., Malato, S., Agüera, A. & Fernández-Alba, A. 2013 Photo-Fenton and modified photo-Fenton at neutral pH for the treatment of emerging contaminants in wastewater treatment plant effluents: a comparison. *Water Research* **47** (2), 833–840.

Konstantinou, I. K., Antonopoulou, M. & Lambropoulou, D. A. 2014 Transformation products of emerging contaminants formed during advanced oxidation processes. In: *Transformation Products of Emerging Contaminants in the Environment* (D. A. Lambropoulou & L. M. L. Nollet, eds). Wiley Online Library, West Sussex United Kingdom, pp. 179–228.

Kumar, S., Nair, R. R., Pillai, P. B., Gupta, S. N., Iyengar, M. & Sood, A. 2014 Graphene oxide–$MnFe_2O_4$ magnetic nanohybrids for efficient removal of lead and arsenic from water. *ACS Applied Materials & Interfaces* **6** (20), 17426–17436.

Li, L., Chen, X., Zhang, D. & Pan, X. 2010 Effects of insecticide acetamiprid on photosystem II (PSII) activity of Synechocystis sp. (FACHB-898). *Pesticide Biochemistry and Physiology* **98** (2), 300–304.

Li, X., Xie, J., Jiang, C., Yu, J. & Zhang, P. 2018 Review on design and evaluation of environmental photocatalysts. *Frontiers of Environmental Science & Engineering* **12** (5), 14.

Liu, Y., Jin, W., Zhao, Y., Zhang, G. & Zhang, W. 2017 Enhanced catalytic degradation of methylene blue by α-Fe_2O_3/graphene oxide via heterogeneous photo-Fenton reactions. *Applied Catalysis B: Environmental* **206**, 642–652.

Luo, W., Zhu, L., Wang, N., Tang, H., Cao, M. & She, Y. 2010 Efficient removal of organic pollutants with magnetic nanoscaled $BiFeO_3$ as a reusable heterogeneous Fenton-like catalyst. *Environmental Science and Technology* **44** (5), 1786–1791.

Mirzaei, A., Chen, Z., Haghighat, F. & Yerushalmi, L. 2017 Removal of pharmaceuticals from water by homo/heterogonous Fenton-type processes–a review. *Chemosphere* **174**, 665–688.

Nadeem, N., Zahid, M., Tabasum, A., Mansha, A., Jilani, A., Bhatti, I. A. & Bhatti, H. N. 2020 Degradation of reactive dye using heterogeneous photo-Fenton catalysts: $ZnFe_2O_4$ and GO-$ZnFe_2O_4$ composite. *Materials Research Express* **7** (1), 015519.

Naushad, M., Ahamad, T., Al-Maswari, B. M., Alqadami, A. A. & Alshehri, S. M. 2017 Nickel ferrite bearing nitrogen-doped mesoporous carbon as efficient adsorbent for the removal of highly toxic metal ion from aqueous medium. *Chemical Engineering Journal* **330**, 1351–1360.

Pérez, M. H., Vega, L. P., Zúñiga-Benítez, H. & Peñuela, G. A. 2018 Comparative degradation of alachlor using photocatalysis and photo-Fenton. *Water, Air, & Soil Pollution* **229** (11), 346.

Pignatello, J. J., Oliveros, E. & MacKay, A. 2006 Advanced oxidation processes for organic contaminant destruction based on the Fenton reaction and related chemistry. *Critical Reviews in Environmental Science and Technology* **36** (1), 1–84.

Qi, H.-P., Wang, H.-L., Zhao, D.-Y. & Wang, X.-K. 2019 Synthesis of novel magnetic superstructure TiO_2 mesocrystal composites with enhanced visible-light photocatalytic activity. *Materials Research Bulletin* **18**, 110516.

Ren, Y., Dong, Q., Feng, J., Ma, J., Wen, Q. & Zhang, M. 2012 Magnetic porous ferrospinel $NiFe_2O_4$: a novel ozonation catalyst with strong catalytic property for degradation of di-n-butyl phthalate and convenient separation from water. *Journal of Colloid and Interface Science* **382** (1), 90–96.

Soto, A. I., Valencia, R. N. A. & Vásquez, A. F. L. 2018 Effect of pH and temperature on photocatalytic oxidation of methyl orange using black sand as photocatalyst. *Mutis* **8** (1), 43–54.

Tabasum, A., Zahid, M., Bhatti, H. N. & Asghar, M. 2019 Fe_3O_4-GO composite as efficient heterogeneous photo-Fenton's catalyst to degrade pesticides. *Materials Research Express* **6** (1), 015608.

Titouhi, H. & Belgaied, J.-E. 2016 Heterogeneous Fenton oxidation of ofloxacin drug by iron alginate support. *Environmental Technology* **37** (16), 2003–2015.

Velichkova, F., Julcour-Lebigue, C., Koumanova, B. & Delmas, H. 2013 Heterogeneous Fenton oxidation of paracetamol using iron oxide (nano)particles. *Journal of Environmental Chemical Engineering* **1** (4), 1214–1222.

Xiang, Q., Yu, J. & Jaroniec, M. 2012 Graphene-based semiconductor photocatalysts. *Chemical Society Reviews* **41** (2), 782–796.

Xu, A., Yang, M., Qiao, R., Du, H. & Sun, C. 2007 Activity and leaching features of zinc–aluminum ferrites in catalytic wet oxidation of phenol. *Journal of Hazardous Materials* **147** (1–2), 449–456.

Yamaguchi, N., Santos, J., Almeida, A., Rubio, A., Junior, N. V., Botassini, M., Nascimento, N. & Bergamasco, R. 2017 Glyphosate removal using reusable ferrite manganese graphene. *Chemical Engineering Transactions* **57**, 685–690.

Yao, Y., Cai, Y., Lu, F., Wei, F., Wang, X. & Wang, S. 2014 Magnetic recoverable $MnFe_2O_4$ and $MnFe_2O_4$-graphene hybrid as heterogeneous catalysts of peroxymonosulfate activation for efficient degradation of aqueous organic pollutants. *Journal of Hazardous Materials* **270**, 61–70.

Yu, L., Chen, J., Liang, Z., Xu, W., Chen, L. & Ye, D. 2016 Degradation of phenol using Fe_3O_4-GO nanocomposite as a heterogeneous photo-Fenton catalyst. *Separation and Purification Technology* **171**, 80–87.

Yu, M., Wang, L., Hu, L., Li, Y., Luo, D. & Mei, S. 2019 Recent applications of magnetic composites as extraction adsorbents for determination of environmental pollutants. *TrAC Trends in Analytical Chemistry* **19**, 015519.

Zahid, M., Nadeem, N., Hanif, M. A., Bhatti, I. A., Bhatti, H. N. & Mustafa, G. 2019 Metal ferrites and their graphene-based nanocomposites: synthesis, characterization, and applications in wastewater treatment. In: *Magnetic Nanostructures* (K. A. Abd-Elsalam, M. A. Mohamed & R. Prasad, eds). Springer, Cham, Switzerland, pp. 181–212.

Zhang, X.-Y., Li, H.-P., Cui, X.-L. & Lin, Y. 2010 Graphene/TiO_2 nanocomposites: synthesis, characterization and application in hydrogen evolution from water photocatalytic splitting. *Journal of Materials Chemistry* **20** (14), 2801–2806.

Zhou, K., Zhu, Y., Yang, X. & Li, C. 2010 One-pot preparation of graphene/Fe_3O_4 composites by a solvothermal reaction. *New Journal of Chemistry* **34** (12), 2950–2955.

Zhou, Y., Xiao, B., Liu, S.-Q., Meng, Z., Chen, Z.-G., Zou, C.-Y., Liu, C.-B., Chen, F. & Zhou, X. 2016 Photo-Fenton degradation of ammonia via a manganese–iron double-active component catalyst of graphene–manganese ferrite under visible light. *Chemical Engineering Journal* **283**, 266–275.

First received 4 September 2019; accepted in revised form 24 February 2020. Available online 3 March 2020